Orientation independent chipless RFID tag using novel trefoil resonators

Tariq, N., Riaz, M., Shahid, H., Khan, M.J., Khan, M.S., Amin, Yasar, Loo, Jonathan ORCID: https://orcid.org/0000-0002-2197-8126 and Tenhunen, H. (2019) Orientation independent chipless RFID tag using novel trefoil resonators. IEEE Access, 7. pp. 122398-122407.

http://dx.doi.org/10.1109/ACCESS.2019.2937131

Orientation Independent Chipless RFID Tag Using Novel Trefoil Resonators

NIMRA TARIQ[1], MUHAMMAD ALI RIAZ[1], (Member, IEEE), HUMAYUN SHAHID[1], (Member, IEEE), MUHAMMAD JAMIL KHAN[1], (Member, IEEE), MANSOOR SHAUKAT KHAN[2], YASAR AMIN[1], (Senior Member, IEEE), JONATHAN LOO[3], (Member, IEEE), AND HANNU TENHUNEN[4,5], (Member, IEEE)

[1]ACTSENA Research Group, Department of Telecommunication Engineering, University of Engineering and Technology, Taxila, Punjab 47050, Pakistan
[2]Mathematics Department, COMSATS University Islamabad, Park Road, Tarlai Kalan, Islamabad 45550, Pakistan
[3]School of Computing and Engineering, University of West London, St Mary's Road, Ealing, W5 5RF, London, United Kingdom
[4]Department of Electronic Systems, Royal Institute of Technology (KTH), Isafjordsgatan 26, Stockholm, SE 16440, Sweden
[5]Department of Information Technology, TUCS, University of Turku, Turku 20520, Finland

Corresponding author: Muhammad Ali Riaz (e-mail: ali.riaz@uettaxila.edu.pk).

ABSTRACT In this paper, a compact and fully passive bit encoding circuit, capable of operating as a chipless radio frequency identification (RFID) tag is presented. The structure consists of novel concentric trefoil-shaped slot resonators realized using Rogers RT/duroid® 5880 laminate, occupying a physical footprint of 13.55 $\times$ 13.55 mm^2. Each resonating element is associated with a particular data bit, having a 1:1 resonator-to-bit correspondence. Bit sequences are configured through introducing modifications in the geometric structure either by addition or exclusion of each nested slot resonator. Such changes manifest directly in the electromagnetic signature of the tag as presence or absence of corresponding resonant peaks. The proposed 10-bit tag offers minimized inter-resonator mutual coupling and insensitivity to changes in polarization and incident angles thereby demonstrating orientation independent functionality. Moreover, error-free encoding is achieved through stabilizing the shift in resonant frequencies for a variety of different geometric configurations and orientation of the structure. The tag operates within the license-free ultra-wideband ranging from 5.4 to 10.4 GHz, providing spectral bit capacity and bit density of 2 bits/GHz and 5.44 bits/cm^2 respectively.

INDEX TERMS Chipless tag, On-Off Keying (OOK), Radar Cross-Section (RCS), Radio Frequency Identification (RFID)

I. INTRODUCTION

RADIO frequency identification (RFID) is an evolving technology for automated recognition of objects through transmitting data using electromagnetic waves [1]. The use of RFID technology has proliferated into numerous applications such as transportation [2], supply chain management [3], logistics [4], and security [5]. Estimated market value for RFID products is expected to reach up to 12 billion dollars by the year 2020 [6]. RFID system generally comprises of two main constituents, 1) RFID tag: carries identification data and is attached to an object, and 2) RFID reader: for transceiving and interpreting data from the RFID tag [7]. Conventional RFID tags consist of an integrated circuit (IC) to carry bit information and an antenna for receiving the interrogating signal and transmitting the stored information using radio frequency waves [8]. The presence of the antenna results in larger size and weight of the tag [9].

The complexity and cost associated with the silicon-chip obstruct the cost-effectiveness of chip-based RFID tags, especially for low-end products [10]. Recently, numerous researchers have proposed chipless RFID tags to overcome the economic constraint associated with the presence of silicon chip [11]–[14]. Eliminating the need for having RF identification chip (RFIC), hence results in a lower cost per tag and simpler production-line processes. Chipless RFID tags are expected to replace the conventional barcode technology primarily due to their inherent characteristics such as lower cost per tag, physical robustness and non-line-of-sight communication [11], [12].

Chipless RFID tags can be classified as time-domain (TD), and frequency-domain (FD) based tags. The surface acoustic wave (SAW) [15] tags are the only commercially available time-domain based tags that make use of the piezoelectric nature of the structure to convert the electromagnetic waves into slower acoustic waves. However, TD SAW tags can only store a limited amount of data [16] and require a complex manufacturing process, hindering their mass adoption. Transmission delay line tags are another category of time-domain based tags based on the capacitive-inductive delay line elements [17]. The data encoded in the tag can be extracted through the reader by analyzing time deferral in the received signal. The size of TD tags [18]–[20] is typically larger than those of chipless RFID tags for a similar number of data bits.

Frequency-domain (FD) based chipless RFID tags are designed such that the encoded data bit is represented as either the presence or absence of a particular resonant frequency. FD tags can further be classified into two categories: 1) retransmission based, and 2) RCS based tags. Retransmission based tags primarily consist of antenna system and a resonant RF circuit. The antenna system transceives the electromagnetic signals, whereas bit information is stored in the circuit [21]. RCS based tags are designed, either to absorb or reflect an impinging electromagnetic wave at different frequencies based on the physical geometry and parameters of the tag. Therefore bit information is stored in the physical geometry of the tag that is reflected in its electromagnetic signature. The electromagnetic response of such tags is measured as the radar cross section (RCS) of the tag with resonances for bit representation [22]–[24].

Recently reported state of the art RCS based chipless RFID tags are mostly based on dipole resonators, such as: capacitively loaded [25], crossed [26], tip loaded [27], and dual-spiral capacitively-loaded [24]. Dipoles are primarily utilized to enhance the spectral bit capacity [25] that ranges from 6.66 [26] to 12.5 [27] bits/GHz for the reported work. However, a trade-off exists between the compactness and spectral bit capacity of the tag. Size of reported dipole based tags varies from 35 $\times$15 mm^2 [27] to 55 $\times$55 mm^2 [24] corresponding to a lower estimated bit density of 0.66 [24] to 1.77 [25] bits/cm^2. Therefore dipole based resonators are unsuitable for chipless RFID tag designs targeted at enhancing bit density. Moreover, such resonators do not offer orientation independent operability since these are polarization sensitive.

RCS based chipless RFID tag incorporating other type of resonators include square loop [28], octagon [29], hybrid circular-square [30], C-section [17] half-wave slot [31], and L-resonator [32]. Although square loop resonators are polarization insensitive, a high inter-resonator mutual coupling is typically observed, limiting the possibility for compactly placing resonators, thus hampering the improvement in bit density. Octagon resonators require repetition of the unit cell to obtain detectable resonances in the RCS. Half-wave slot resonators carry similar characteristics to those of dipole resonators and are more suitable for achieving higher spectral bit capacity at the cost of lowered bit density. Although L-resonator based chipless RFID tags offer high bit density and spectral bit capacity of 18 bits/cm^2 and 12 bits/GHz, the design is not orientation independent.

In this work, a novel trefoil-shaped slot resonator based chipless RFID tag is presented. The proposed design offers compactness demonstrated through a bit density of 5.44 bits/cm^2. Furthermore, a bit capacity of 2 bits/GHz is also attained having a bit capacity of 10 bits. The presented novel resonator design offers minimized inter-resonator coupling allowing for close placement of slot resonators. Error-free bit encoding for different bit sequences is also achieved through stabilized frequency response of the resonator design under different conditions of presence or absence of neighbouring elements. The tag occupies a physical footprint of 13.55 $\times$ 13.55 mm^2 and covers the license free UWB of 5.4-10.4 GHz. Functional prototypes are realized on Rogers RT/duroid® 5880 laminate and measurements are carried out to analyze the electromagnetic performance of the proposed tag.

II. RESONANT ELEMENT DESIGN

Geometric structure of a single compact, trefoil-shaped slot resonator along with its parameters are presented in Fig. 1. Three circles are utilized in designing a single resonator. The diameter D_a of the above circle is a bit larger than the others represented by D_b. Consequently, the addition of three circles results in the basic resonant element design.

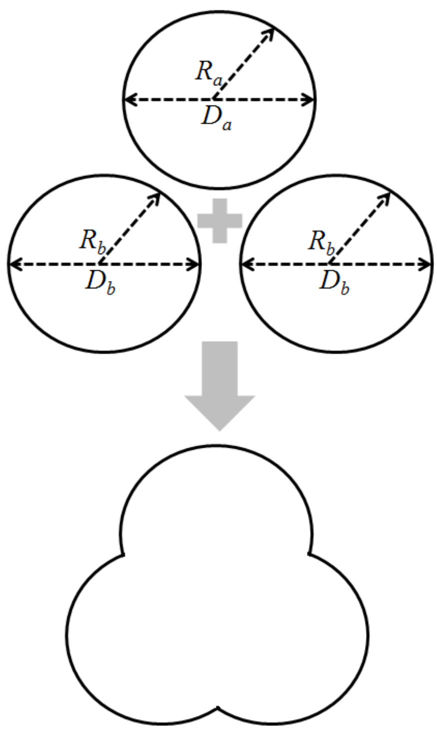

FIGURE 1: Basic resonant element geometric structure.

A single trefoil shaped slot resonator is realized on Rogers RT/duroid® 5880 with a thickness of 1.575 mm and relative permittivity of 2.2. A trefoil slot is designed on compact tag dimensions of 13.55 $\times$ 13.55 mm^2, as illustrated in

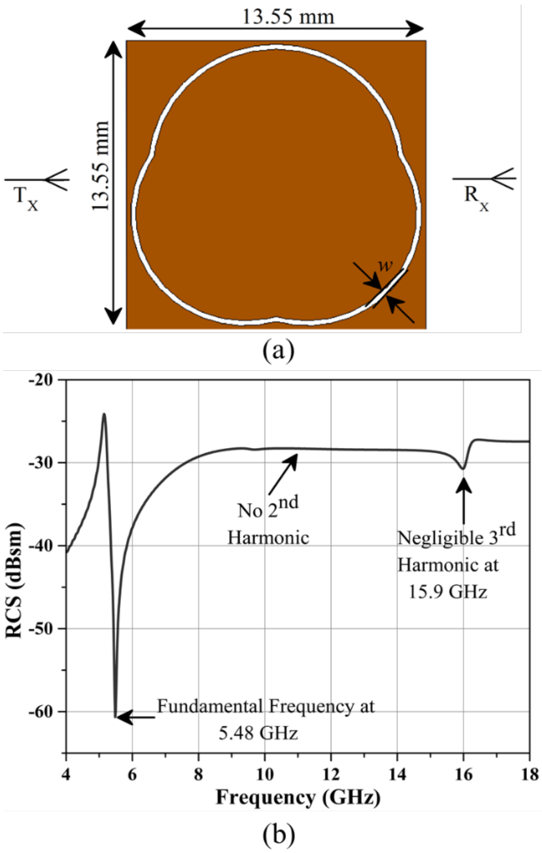

FIGURE 2: (a) Geometry of trefoil shaped resonator and (b) RCS response.

Fig. 2 (a). The width of slot is defined by parameter w while maintaining a finite distance from the outer boundary. Moreover, the proposed tag does not contain any ground plane since the design is a slot based resonator that is etched from a square metallic patch having a thickness of 35 μm. The optimized values for the circular components of slot are given by D_a and D_b as 5.8 mm and 5.2 mm respectively, while slot thickness w is kept at 0.2 mm.

The chipless RFID tag is excited using a linearly polarized electromagnetic wave. The instantaneous E-field incident plane wave, travelling in the z direction is mathematically provided in [33]. The relationship between RCS response of the tag to the scattered (E_{scat}) and incident (E_{inc}) electric field intensity [34] is given in Equation 1.

$$\sigma = \lim_{r \to \infty} \left[4\pi r^2 \frac{|E_{scat}|^2}{|E_{inc}|^2} \right] \tag{1}$$

Here σ is the RCS magnitude, r is the distance between the tag and interrogating antenna. Since RCS is a far field parameter [35], it must be observed at a distance provided by r in Equation 2.

$$r \geq \frac{2D^2}{\lambda} \tag{2}$$

Here, D represents the largest dimensions of the tag and λ signifies the wavelength of the electromagnetic wave.

The electromagnetic performance of the proposed single trefoil slot resonator is scrutinized using CST® Microwave Studio Suite®. The slot resonator present on the tag resonates at its particular frequency and absorbs [36] the impinging signal after being illuminated by the frequency-swept linearly polarized incident wave. Such absorption characteristics can be observed as presence of a spectral dip in the RCS response of the circuit as illustrated in Fig. 2 (b) at 5.48 GHz. In the case of no resonance, the signal is reflected at the reader. Reflection characteristics can be observed in Fig. 2 (b) at such frequencies where resonant peaks in the RCS response are absent.

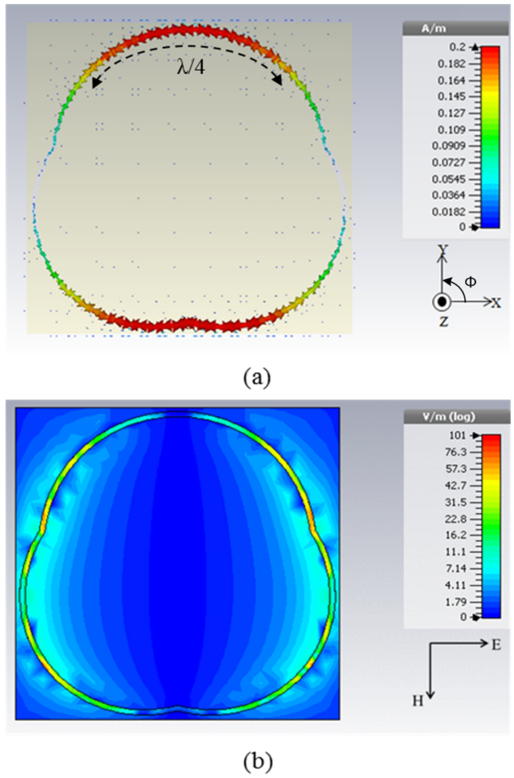

FIGURE 3: (a) Surface current distribution and (b) electric field intensity of trefoil resonator at 5.48 GHz.

Frequency selective surface (FSS) repetitions are not essential for this design, resulting in a 1:1 resonator to bit correspondence. Such characteristics allow for the tag design to be fairly compact [37]. The proposed resonant design exhibits no 2nd harmonic and a negligible 3rd harmonic, eliminating the presence of spurious peaks within a wide range of frequencies [38].

Fig. 3 (a) depicts the surface current distribution of trefoil resonator at its fundamental frequency of 5.48 GHz. The top and the bottom part of the slot is concentrated by the surface current, implying the occurrence of an inductive behavior. Whereas, the distribution of surface current density is relatively lower on the left and right side of the trefoil structure: indicating a capacitive characteristic. The simultaneous existence of capacitive and inductive distribution along a trefoil slot resonator instigates a resonance at a distinct frequency of 5.48 GHz.

The distribution of electric field, on the other hand, is shown in Fig. 3 (b). Minimum intensity is observed on the top and lower bottom of the trefoil structure. Relatively higher E-field intensity is present at the left and right side of the structure. Such profile of the surface current distribution and electric field intensity at resonance demonstrates the creation of a standing wave mode at resonance. Moreover, the resonance of $\lambda/4$ is proven throughout the simulation process using CST® MWS® as shown in Fig. 3(a).

The peculiar geometry of the slot resonator not only minimizes the harmonic effects but also makes the resonant design polarization insensitive. The RCS magnitude response of radiating element at various polarization angles is shown in Fig. 4. As the polarization angle increases, overall RCS magnitude response attenuates while a slight displacement in the resonant frequency occurs, demonstrating an overall angular stability of the design.

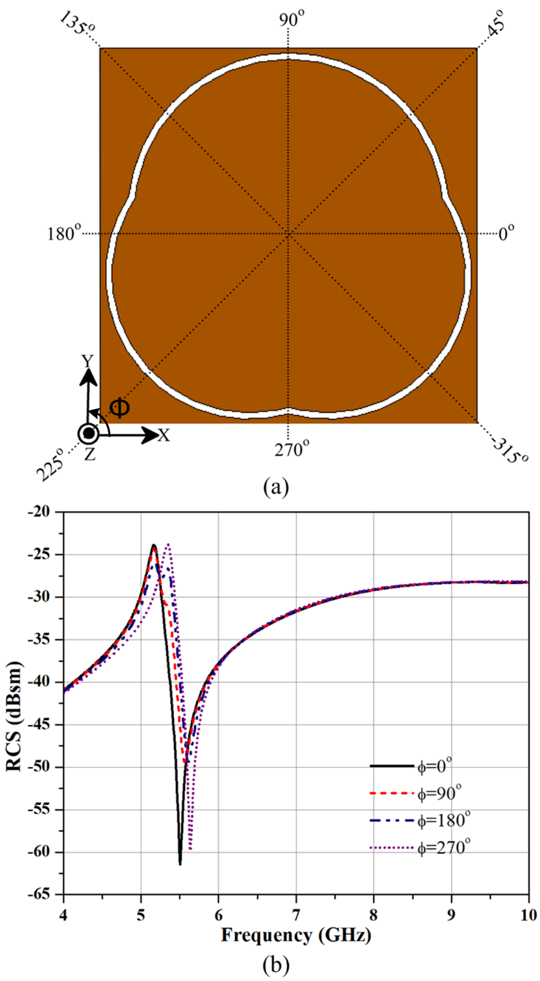

FIGURE 4: Variation in RCS performance at various polarization angles.

III. OVERALL TAG DESIGN

The tag is designed using a loop based strategy. Nesting technique is employed by introducing additional small-sized trefoil resonators within the larger one. Employing this technique not only decreases the overall footprint of the tag but also enhances the code density. There are ten nested slot based resonators corresponding to 10 bits generating 2^{10} possible tag ID combinations. Each slot is numbered according to the bit position.

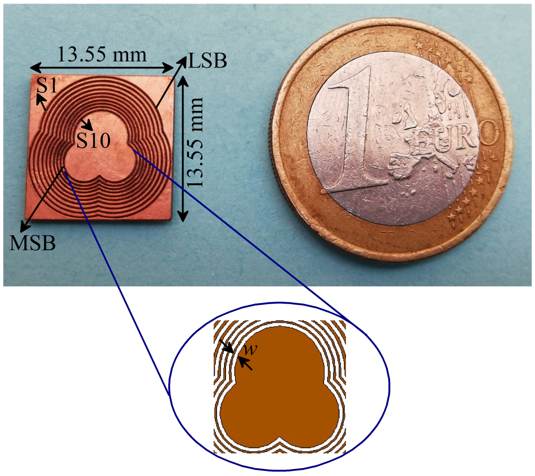

FIGURE 5: Fabricated prototype of 10 bit proposed tag.

The compact size of the tag is endorsed by placing the realized tag beside a euro coin as shown in Fig. 5. Henceforth, the proposed tag is conveniently compact and minuscule. The smallest slot element resonates at maximum frequency indicated as most significant bit (MSB). While the largest slot element resonates at the minimum frequency indicated as least significant bit (LSB). Additional radiating elements may be introduced on the outer side of the tag by increasing its surface area at the cost of lower bit density. Moreover, addition of smaller elements corresponding to resonances at higher frequencies tends to reduce the spectral bit capacity of the tag. The inter-slot spacing is provided in Table 1.

TABLE 1: Inter-slot spacing

Slot	Inter-slot gap
S1-S4	0.2 mm
S4-S7	0.15 mm
S7-S10	0.1 mm

Precise geometric parameters of the resonators conforming to each bit location are listed in Table 2. The dimensions are selected carefully through parametric analysis to ensure high code density and spectral bit capacity that enables the accommodation of ten resonances in the spectral range of 5 GHz to 10.4 GHz. ON-OFF Keying (OOK) is employed to encode different bit sequences.

TABLE 2: Geometric parameters of trefoil slot resonator

Bit postion	S1	S2	S3	S4	S5	S6	S7	S8	S9	S10
D_a (mm)	6.6	6.2	5.8	5.4	5.05	4.75	4.45	4.15	3.85	3.55
D_b (mm)	5.5	5.1	4.7	4.3	3.95	3.65	3.35	3.05	2.75	2.45

The removal or addition of each slot element results in the absence or presence of resonating bit respectively. Removal of a bit is represented by logic '0' while the presence of a bit is represented by logic '1'. The backscattered signal containing this bit information is captured through the receiving antenna of the reader, signifying the presence of resonant peaks as bit '1' and vice versa.

IV. RESULTS AND DISCUSSION

This section demonstrates the computed and measured results for the electromagnetic performance of presented chipless RFID tag. CST® Microwave Studio® is used to perform the computer-based simulation and optimization of the presented tag. The RCS response of the bit words 1111111111, 1010101011, 1010101100 and all zeros is investigated and shown in Fig. 6.

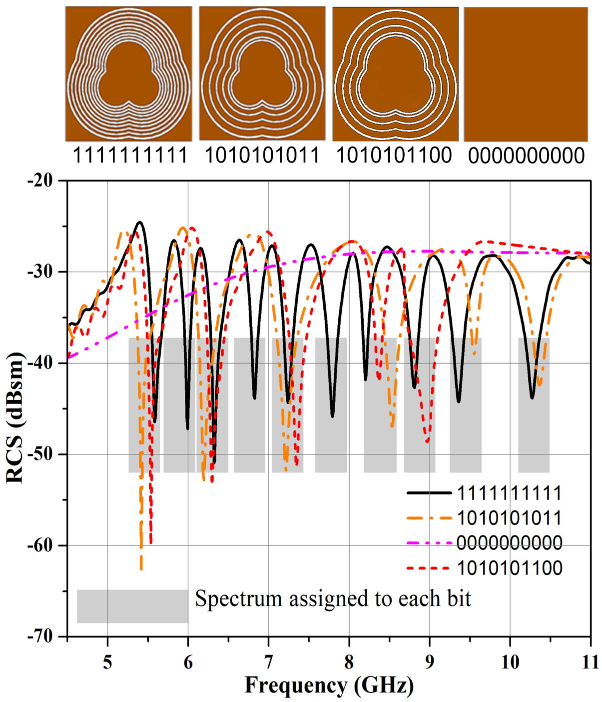

FIGURE 6: Simulated RCS response for different bit combinations.

The backscattered frequency signature with ten distinct resonances is obtained through geometric repetition of the same number of trefoil elements in a unit cell resulting in a 1:1 resonator to bit correspondence. Whereas, the absence of trefoil resonator in the structure causes exclusion of its corresponding resonance in the RCS response of the tag. A small drift along frequency axis can be observed for different random sequences when compared with all one's. This shift specifies the dependence of resonator on its physical parameters and mutual coupling effects of nearby resonant elements. Thus, a spectral band of 250 MHz is allocated to each resonating bit to avoid false detection of the bit as specified by a shaded region in Fig. 6. Minimal mutual coupling is observed primarily due to two phenomena: 1) There is a 1:1 resonating element to bit correspondence 2) the frequency shift due to absence or presence of neighboring elements is small, and resonances stay with their assigned frequency band.

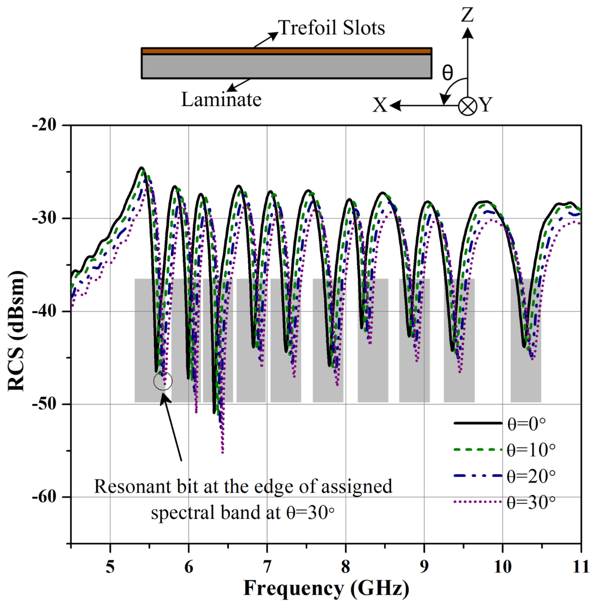

FIGURE 7: Oblique incidence performance for all 1's sequence.

The gap between the resonators is chosen to enhance the spectral bit capacity of the proposed tag while limiting the coupling characteristics. Therefore the spectral limit assigned to each bit is taken into consideration to avoid overlapping with nearby spectral dips and detection of incorrect bit position. Fig. 7 reports the RCS response of the formulated chipless RFID tag for all 1's sequence at different oblique incident angles. All resonances stay within their assigned frequency band while operating in leaning position with respect to the reader. As the incident angle is changed, a slight displacement in the resonant frequencies is noticed with an overall downward trend in the RCS magnitude. The analysis demonstrates the tag's operability for incident angles up to 30° because the resonant bit near 5 GHz appears at the edge of its predefined spectral band.

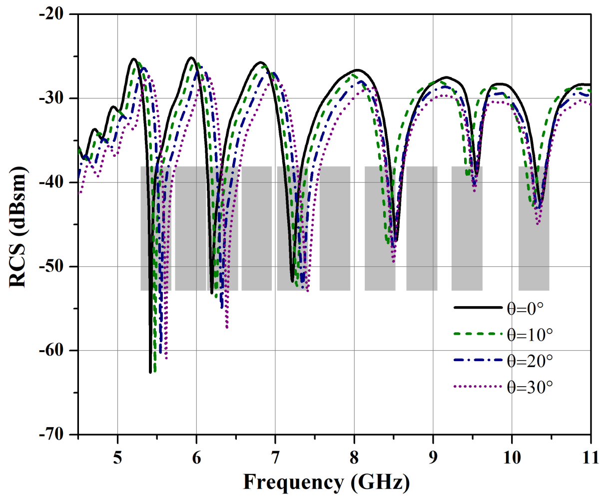

FIGURE 8: Oblique incidence performance for 1010101011 sequence.

The oblique incidence performance for a different bit sequence is shown in Fig. 8. Although, some resonances appear to be on the edges of the corresponding spectrums, the resonances stay within their corresponding limits. This demonstrates the readability of the tag at a varierty of incident angles for a different bit sequence. The polarization insensitivity of the tag is demostrated in Fig. 9. It is evident that all resonances are present with no spurious peaks and stay within the defined spectral bands.

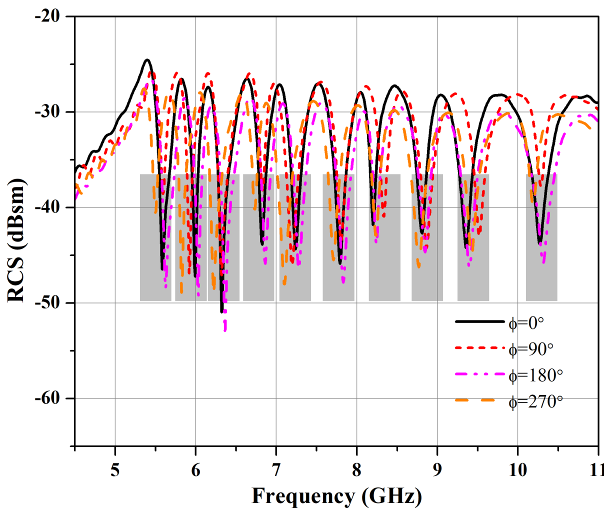

FIGURE 9: Performance of the tag at different polarization angles.

The realized tag samples are analyzed for their real-world performance using well-known far-field RCS measurement setup. The arrangement used in this work is the same as the one utilized in [39], [40], and is illustrated in Fig. 10 having a combination of similar transmitting and receiving horn antennas, vector network analyzer (VNA) R&S®, ZVL-13 and the tag prototype under test. The transmitting antenna is used to transmit the incident electromagnetic wave towards the tag. The backscattered signal from the tag with encoded information is captured by the receiving horn antenna. Transmitting and receiving antennas are connected to each port of the VNA that analyzes the S_{21} parameter. Transmit power of 0 dBm is used for the frequency range from 5.4 to 10.4 GHz. The tag is placed at a distance of 35 cm from the interrogating horn antennas within the far-field region. Since VNA is used to measure the scattering parameters, Equation 3 is employed to estimate the measured RCS of the tag [41].

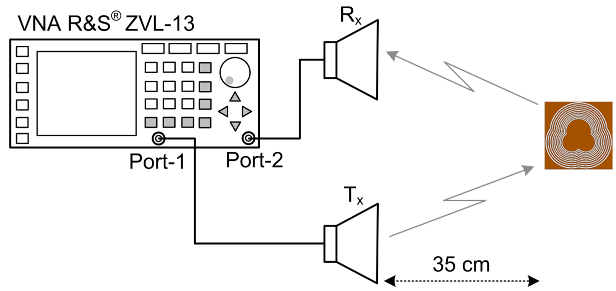

FIGURE 10: Block diagram of tag measurement setup.

$$\sigma^{tag} = \left[\frac{S_{21}^{tag} - S_{21}^{isolation}}{S_{21}^{ref} - S_{21}^{isolation}}\right]^2 \sigma^{ref} \qquad (3)$$

where σ^{ref} is the RCS of an object that is already known, such as that of a rectangular metal plate. S_{21}^{tag} is obtained in the presence of the chipless RFID tag. The procedure also incorporates for calibration since $S_{21}^{isolation}$ is measured in the absence of chipless RFID tag to eliminate unwanted environmental effects in measured RCS.

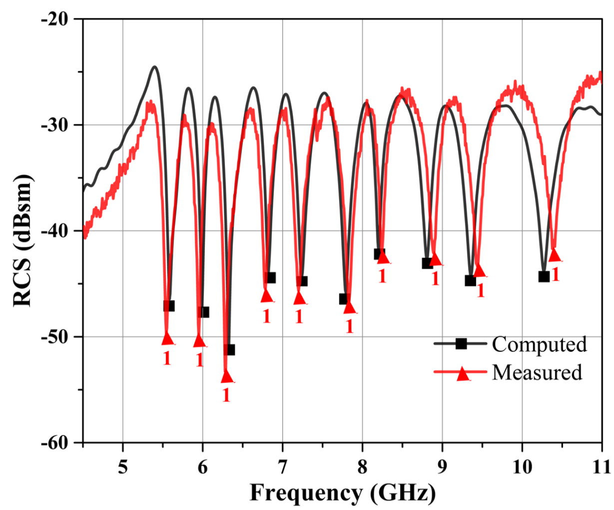

FIGURE 11: Measured and simulated results of tag for all 1's spectral dips.

Computed and measured results of the proposed chipless RFID tag having all 1's bit configuration are compared in Fig. 11. A small shift in few resonant dips along the spectral axis is observed which is caused by the physical imperfection of realized tag introduced over the fabrication process. RCS response of all drifted resonances is visually distinct with sufficient absorption level. As depicted, FSS structural repetition is not required resulting in a miniaturized tag design. Moreover, experimental and measured results do not manifest a spurious dip: resulting in error-free encoding.

Fig. 12 shows the measured and computed RCS response for alternating bit sequence tag. Absence of slot resonator causes the corresponding resonance to disappear, enabling the possibility of encoding a random bit sequence. It can be seen that the electromagnetic absorption level of radiating slots resonate at low-frequencies is increased, with the omission of their nearby elements. Although the resonance peaks along the frequency axis are slightly shifted with variation in mutual coupling, yet no other significant discrepancies such as spurious radiations are noticed.

The measured RCS response for 10-bit tag encoding different bit sequence 1111111111, 1010101011, 1010101010 and all zero's is presented in Fig. 13. The shaded assigned spectral bands only correspond to the frequency axis. It is worth mentioning here that the shaded bands do not correspond to the RCS level. As stated earlier, a subtle drift in resonances along the frequency axis is observed due to the mutual coupling among resonators as well as slight structural infirmity introduced during the fabrication process. Besides, the drift does not exceed the frequency spectrum assigned to each bit. Meanwhile, the resonant frequencies operate agreeably within the specified spectrum band, and it can easily be detected by calculating the variation in local minima to local maxima of RCS profile. The measured RCS minima for the proposed chipless RFID tag design hover around -50 dBsm or below and variations at such RCS levels also need to be observed for accurate bit detection. Therefore, a distance

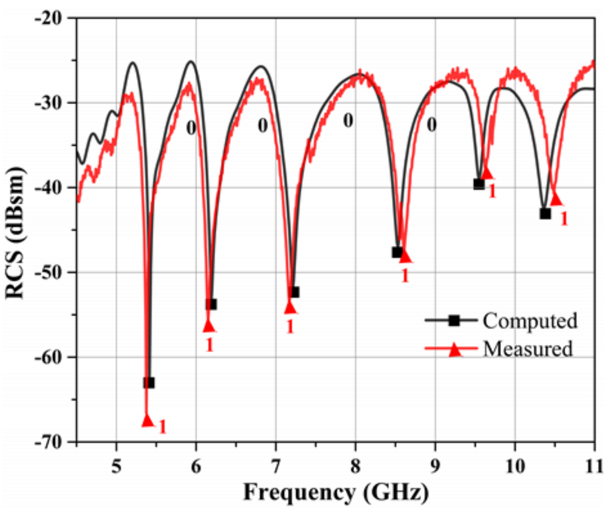

FIGURE 12: Measured and simulated results of tag for a random bit sequence.

of 35 cm was chosen to accommodate detection of such RCS levels. Moreover, a transmit power of 0 dBm is used with the gain of similar T_x and R_x antennas ranging from 10 dBi to 13 dBi for the operational frequency band.

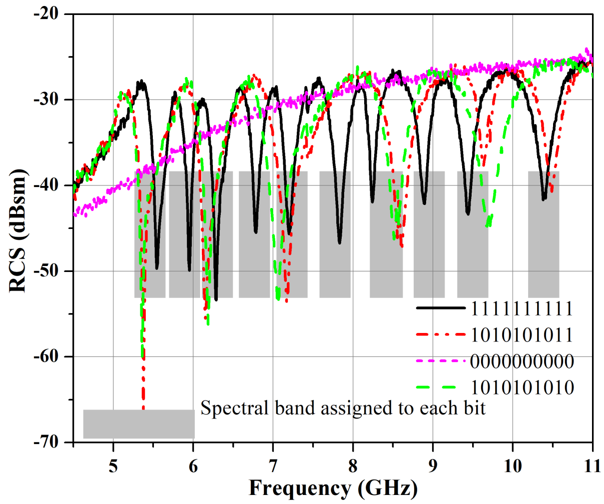

FIGURE 13: Measured RCS response for different bit sequences.

The RCS response of the proposed trefoil shaped tag at different polarization angles is depicted in Fig. 14. It can be noticed that as polarization angle changes, a slight displacement occurs both in resonant frequencies and RCS magnitude response over the frequency band. However, the corresponding resonances stay within the limits of their assigned frequency bands. Therefore, the proposed tag design is polarization insensitive making it valuable in practical utilization.

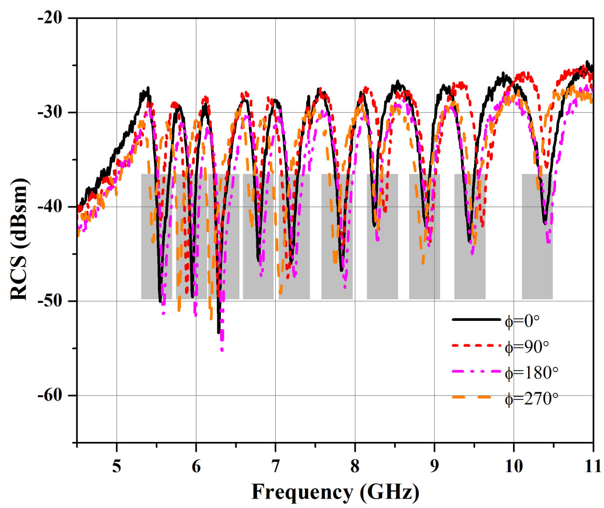

FIGURE 14: Measured RCS response of the tag at different polarization angles.

Table 3 compares the proposed work with other state-of-the-art tags based on various performance parameters, such as tag dimensions, bit density, spectral bit capacity,

TABLE 3: Comparison with other state of the art designs

Resonator	Tag Dimensions (mm^2)	Bit Capacity (Bits)	Bit Density ($bits/cm^2$)	Spectral Bit Capacity (Bits/GHz)	Orientation Independence	Frequency Range (GHz)	Resonant Stability	Printable
C-loaded Dipole [25]	17 × 68	20	1.77	12.50	No	2.0–3.6	Yes	Yes
Crossed Dipole [26]	45 × 45	20	0.98	6.67	No	2.0–5.0	N.C.	Yes
Tip-Loaded Dipole [27]	35 × 15	04	0.76	12.50	No	3.2–3.6	N.C.	Yes
DS CLD [24]	55 × 55	20	0.66	12.50	No	1.8–3.6	Yes	Yes
Square Loop [28]	15 × 15	05	2.22	1.25	Yes	5.5–9.5	Yes	Yes
Octagon [29]	52 × 82	05	0.18	0.63	Yes	2.0–10.0	Yes	Yes
Circular-Square [30]	20 × 40	28.5	3.56	3.80	N.C.	3.1–10.6	Yes	Yes
C-section [17]	100 × 55	43	0.78	5.8	No	3.1–10.6	N.C.	Yes
Half-Wave Slot [31]	36 × 36	21	0.88	7.00	No	1.7–4.7	N.C.	Yes
L-resonator [32]	15 × 10	18	12	3.46	No	4.8–10.0	Yes	Yes
Trefoil (This Work)	13.55 × 13.55	10	5.44	2.00	Yes	5.4–10.4	Yes	Yes

*N.C: Not Considered

orientation independence, etc. Design strategies for chipless RFID tags are primarily focused on either enhancing the bit density ($bits/cm^2$) or spectral bit capacity (bits/GHz). Resonators such as C-loaded, crossed, tip-loaded, DS CLD dipoles, and half wave slot offer higher spectral bit capacity. Whereas, such resonators are typically larger, have lesser bit density, and exhibit polarization sensitivity. The square loop resonator has a comparatively higher bit density as compared to dipoles and half wave slot; it has low spectral bit capacity. The L-resonator demonstrates a high bit density and spectral bit capacity, however it lacks orientation independent features. The novel trefoil resonator based chipless RFID tags offers 10 bits of capacity within a compact footprint of 13.55×13.55 mm^2. It offers a bit density of 5.44 $bits/cm^2$ with a spectral bit capacity of 2 bits/GHz. Moreover, the tag is readable at a variety of orientations, offers resonant stability, and is fully printable.

V. CONCLUSION

A compact, fully passive, trefoil-resonator based chipless RFID tag has been proposed in this paper. The resonator design has been evaluated for presence of unwanted harmonic resonances, polarization insensitivity, and sufficient RCS absorption levels. The overall tag design has been realized using Rogers RT/duroid® 5880 laminate and its performance was examined through electromagnetic simulations and measurements. Design compactness has been achieved through close placement of nested resonators while ensuring minimized effects of mutual coupling in the spectral domain. Resonant stability has also been analyzed concerning changes in mutual coupling for different tag IDs and a variety of oblique incident angles. The tag demonstrates the ability to encode a large number of bits within a compact footprint while offering orientation independence, resonant stability, and full printability of the design.

REFERENCES

[1] H. Shan, J. Peterson III, S. Hathorn and S. Mohammadi,"The RFID Connection: RFID Technology for Sensing and the Internet of Things," *IEEE Microw. Mag.*, vol. 19, no. 7, pp. 63–79, Nov.–Dec. 2018.

[2] D. Inserra, W. Hu and G. Wen, "Antenna Array Synthesis for RFID-Based Electronic Toll Collection," *IEEE Trans. Antennas Propag.*, vol. 66, no. 9, pp. 4596–4605, Sept. 2018.

[3] S. Mondal, K. P. Wijewardena, S. Karuppuswami, N. Kriti, D. Kumar and P. Chahal, "Blockchain Inspired RFID-Based Information Architecture for Food Supply Chain," *IEEE Internet Things J.*, vol. 6, no. 3, pp. 5803-5813, June 2019.

[4] Y. Rouchdi, A. Haibi, K. El Yassini, M. Boulmalf and K. Oufaska, "RFID Application to Airport Luggage Tracking as a Green Logistics Approach," in *2018 IEEE 5th Int. Congr. Inf. Sci. and Technol. (CiSt)*, Marrakech, 2018, pp. 642-649.

[5] C. Herrojo, J. Mata-Contreras, A. Núñez, F. Paredes, E. Ramon and F. Martín, "Near-Field Chipless-RFID System With High Data Capacity for Security and Authentication Applications," *IEEE Trans. Microw. Theory Techn.*, vol. 65, no. 12, pp. 5298-5308, Dec. 2017.

[6] R. Das, "RFID Forecasts, Players and Opportunities 2018-2028: The complete analysis of the global RFID industry," IDTechEx, Cambridge, MA, Tech. Rep, Nov. 2018. [Online]. Available: www.IdtechEx.com

[7] A. Lozano-Nieto, "Basic Principles of Radiofrequency Identification," in *RFID Design Fundamentals and Applications.* Boca Raton, FL, USA: Taylor & Francis, 2010, pp. 5–6.

[8] U.H. Khan, B. Aslam, J. Khan, M. Nadeem, H. Shahid, M.A. Azam, Y. Amin, and H. Tenhunen, "A Novel Asterisk-Shaped Circularly Polarized RFID Tag for On-Metal Applications," *Appl. Comput. Electromagn. Soc. J.*, vol. 31, no. 9, 2016.

[9] S. Dey, J. K. Saha and N. C. Karmakar, "Smart Sensing: Chipless RFID Solutions for the Internet of Everything," *IEEE Microw. Mag.*, vol. 16, no. 10, pp. 26–39, Nov. 2015.

[10] N. C. Karmaker, "Tag, You're It Radar Cross Section of Chipless RFID Tags," *IEEE Microw. Mag.*, vol. 17, no. 7, pp. 64–74, July 2016.

[11] S. Preradovic, and N.C. Karmakar, "Low cost chipless RFID systems," in *Multiresonator-Based Chipless RFID*, Springer, New York, 2012, pp. 9–24.

[12] S. Preradovic and N. C. Karmakar, "Chipless RFID: Bar Code of the Future," *IEEE Microw. Mag.*, vol. 11, no. 7, pp. 87–97, Dec. 2010.

[13] N.C. Karmakar, M. Zomorrodi, and C. Divarathne, *Advanced Chipless RFID: MIMO-Based Imaging at 60 GHz-ML Detection*, John Wiley & Sons, vol. 1187, 2016.

[14] M. M. Khan, F. A. Tahir and H. M. Cheema, "High capacity polarization sensitive chipless RFID tag," in *2015 IEEE Int. Symp. Antennas and Propag. & USNC/URSI Nat. Radio Sci. Meeting*, Vancouver, BC, 2015, pp. 1770–1771.

[15] V. P. Plessky and L. M. Reindl, "Review on SAW RFID tags," *IEEE Trans. Ultrason., Ferroelectr., Freq. Control*, vol. 57, no. 3, pp. 654–668, March 2010.

[16] F. Costa, S. Genovesi and A. Monorchio, "Normalization-Free Chipless RFIDs by Using Dual-Polarized Interrogation," *IEEE Trans. Microw. Theory Techn.*, vol. 64, no. 1, pp. 310-318, Jan. 2016.

[17] R. S. Nair and E. Perret, "Folded Multilayer C-Sections With Large Group Delay Swing for Passive Chipless RFID Applications," *IEEE Trans. Microw. Theory Techn.*, vol. 64, no. 12, pp. 4298-4311, Dec. 2016.

[18] A. Chamarti and K. Varahramyan, "Transmission Delay Line Based ID Generation Circuit for RFID Applications," *IEEE Microw. Wireless Compon. Lett.*, vol. 16, no. 11, pp. 588–590, Nov. 2006.

[19] L. Zheng, S. Rodriguez, L. Zhang, B. Shao and L. Zheng, "Design and implementation of a fully reconfigurable chipless RFID tag using Inkjet printing technology," in *2008 IEEE Int. Symp. on Circuits and Syst.*, Seattle, WA, 2008, pp. 1524-1527.

[20] M. Schubler, C. Mandel, M. Maasch, A. Giere and R. Jakoby, "Phase modulation scheme for chipless RFID- and wireless sensor tags," in *2009 Asia Pacific Microw. Conf.*, Singapore, 2009, pp. 229–232.

[21] M. A. Ashraf et al., "Design and Analysis of Multi-Resonators Loaded Broadband Antipodal Tapered Slot Antenna for Chipless RFID Applications," *IEEE Access*, vol. 5, pp. 25798-25807, 2017.

[22] M. Polivka, J. Havlicek, M. Svanda and J. Machac, "Improvement in Robustness and Recognizability of RCS Response of U-Shaped Strip-Based Chipless RFID Tags," *IEEE Antennas Wireless Propag. Lett.*, vol. 15, pp. 2000-2003, 2016.

[23] R. A. A. Rodrigues, E. C. Gurjão and F. M. de Assis, "Radar cross-section and electric field analysis of backscattering elements of chipless RFID tag," in *2014 IEEE RFID Technol. and Appl. Conf. (RFID-TA)*, Tampere, 2014, pp. 103–108.

[24] M. Svanda, J. Havlicek, J. Machac and M. Polivka, "Polarisation independent chipless RFID tag based on circular arrangement of dual-spiral capacitively-loaded dipoles with robust RCS response," *IET Microw., Antennas & Propag.*, vol. 12, no. 14, pp. 2167-2171, 2018.

[25] J. Havlicek, M. Svanda, M. Polivka, J. Machac and J. Kracek, "Chipless RFID Tag Based on Electrically Small Spiral Capacitively Loaded Dipole," *IEEE Antennas Wireless Propag. Lett.*, vol. 16, pp. 3051-3054, 2017.

[26] M. Khaliel, A. El-Awamry, A. Fawky Megahed and T. Kaiser, "A Novel Design Approach for Co/Cross-Polarizing Chipless RFID Tags of High Coding Capacity," *IEEE J. Radio Freq. Identif.*, vol. 1, no. 2, pp. 135-143, June 2017.

[27] A. M. J. Marindra and G. Y. Tian, "Chipless RFID Sensor Tag for Metal Crack Detection and Characterization," *IEEE Trans. Microw. Theory Techn.*, vol. 66, no. 5, pp. 2452-2462, May 2018.

[28] N. Chen, Y. Shen, G. Dong and S. Hu, "Compact Scalable Modeling of Chipless RFID Tag Based on High-Impedance Surface," *IEEE Trans. Electron Devices*, vol. 66, no. 1, pp. 200-206, Jan. 2019.

[29] D. Betancourt, K. Haase, A. Hübler and F. Ellinger, "Bending and Folding Effect Study of Flexible Fully Printed and Late-Stage Codified Octagonal Chipless RFID Tags," *IEEE Trans. Antennas Propag.*, vol. 64, no. 7, pp. 2815-2823, July 2016.

[30] M. M. Khan, F. A. Tahir, M. F. Farooqui, A. Shamim and H. M. Cheema, "3.56-bits/cm^{2}Compact Inkjet Printed and Application Specific Chipless RFID Tag," *IEEE Antennas Wireless Propag. Lett.*, vol. 15, pp. 1109-1112, 2016.

[31] Y. Chen, T. Jiang and F. Lai, "Automatic Topology Generation of 21 Bit Chipless Radio Frequency Identification Tags Using a Noniterative Technique," *IEEE Antennas Wireless Propag. Lett.*, vol. 18, no. 2, pp. 293-297, Feb. 2019.

[32] K. Issa, M. A. Ashraf, M. R. AlShareef, H. Behairy, S. Alshebeili, and H. Fathallah, "A Novel L-Shape Ultra Wideband Chipless Radio-Frequency Identification Tag," *Int. J. of Antennas and Propag.*, vol. 2017, 2017.

[33] C. A. Balanis, "Fundamental Parameters and Figures-of-Merit of Antennas," in *Antenna Theory Analysis and Design.*, 4th ed., Hoboken, NJ, USA: John Wiley & Sons, 2016, pp. 68–69.

[34] O. Rance, E. Perret, R. Siragusa, "Theory of Chipless RFID Tags," in *RCS Synthesis for Chipless RFID: Theory and Design.*, Kidlington, Oxford, UK: Elsevier, 2017, pp. 53–54.

[35] C. A. Balanis, "Auxiliary Vector Potentials, Construction of Solutions, and Radiation and Scattering Equations," in *Advanced Engineering Electromagnetics.*, 2nd ed., Hoboken, NJ, USA: John Wiley & Sons, 2012, pp. 287–288.

[36] F. Costa, S. Genovesi and A. Monorchio, "A Chipless RFID Based on Multiresonant High-Impedance Surfaces," *IEEE Trans. Microw. Theory Techn.*, vol. 61, no. 1, pp. 146-153, Jan. 2013.

[37] R. Dinesh, P. V. Anila, C. M. Nijas, M. Sumi and P. Mohanan, "Modified open stub multi-resonator based chipless RFID tag," in *2014 URSI General Assem. and Scientific Symp. (URSI GASS)*, Beijing, 2014, pp. 1-4.

[38] M. Martinez and D. van der Weide, "Compact slot-based chipless RFID tag," in *2014 IEEE RFID Technol. and Appl. Conf. (RFID-TA)*, Tampere, 2014, pp. 233-236.

[39] H. Anam, A. Habib, S. I. Jafri, Y. Amin, H. Tenhunen "Directly Printable Frequency Signatured Chipless RFID Tag for IoT Applications," *Radioengineering*, vol. 26, no. 1, pp. 139–146, 2017.

[40] A. Zahra, H. Shahid, M. A. Riaz, Y. Amin, H. Tenhunen, "A chipless RFID tag for smart temporal applications," *Int. J. RF Microw. Comput. Aided Eng.*, vol. 28, no. 8, pp. e21405, 2018.

[41] E. Perret, "Development of Chipless RFID," in *Radio Frequency Identification and Sensors: From RFID to Chipless RFID.*, Hoboken, NJ, USA: John Wiley & Sons, 2014, pp. 140–141.

NIMRA TARIQ received her BS degree in Telecommunication Engineering from the University of Engineering and Technology, Taxila, Pakistan in 2016. She joined the same institute in 2017, where she is pursuing her MS degree focusing on chipless RFID tags, under the supervision of Engr. M. Ali Riaz. She is currently working as a full-time research scholar with the ACTSENA research group.

MUHAMMAD ALI RIAZ received his B.S. and M.S. degree in Electrical Engineering from Iowa State University, USA in 2010 and 2009 respectively. Afterwards, he joined the Department of Electrical and Computer Engineering, Iowa State University, USA as a Research Assistant. He received his Ph.D. degree in Telecommunication Engineering from University of Engineering and Technology, Taxila, Pakistan in 2019. He is currently serving as Assistant Professor associated with ACTSENA research group at University of Engineering and Technology, Taxila. Ali is working towards the design and implementation of chipless RFID tags based on electromagnetic signature and their signal processing applications. He also serves as the director of Electronics and Measurements laboratory at his department. His research work has been featured in a number of ISI-indexed journals.

HUMAYUN SHAHID received his BS degree in Communication Systems Engineering from the Institute of Space Technology, Islamabad in 2008. He joined Space and Upper Atmosphere Research Commission (SUPARCO) where he worked on radiation-hardened space grade components for telemetry subsystems. In 2011, Humayun completed his MS in Signal Processing from Nanyang Technological University, Singapore. Thereafter, he joined the department of telecommunication engineering at the University of Engineering and Technology, Taxila where he currently works as an Assistant Professor. Humayun is affiliated with the ACTSENA research group working towards design and signal processing-related aspects of electromagnetic transduction-based sensor-incorporated chipless RFID tags. He is also the director at the departmental Antenna and RF laboratory. His research work has been featured in a number of ISI-indexed journals and international conferences.

This article has been accepted for publication in a future issue of this journal, but has not been fully edited. Content may change prior to final publication. Citation information: DOI 10.1109/ACCESS.2019.2937131, IEEE Access

MUHAMMAD JAMIL KHAN received the B.Sc. Engineering degree in Computer Engineering, The M.Sc. degree in Telecommunication Engineering, and the Ph.D. degree in Computer Engineering from University of Engineering and Technology, Taxila, Pakistan, in 2005, 2009 and 2016 respectively. He is currently Assistant Professor and director of Embedded Systems and Digital Signal Processing Laboratory in the same University. He is also the founder of Virtual Reality Simulation Laboratory at the University. He has authored or co-authored numerous technical articles in well-known international journals and conferences. His current research interests include multimedia content analysis, RF identification and machine learning.

MANSOOR SHAUKAT KHAN received his B.Sc. degree from PU Lahore, Pakistan in 1994, M.Sc. degrees in Statistics from University of ARID Agriculture Rawalpindi, Pakistan in 2000. He received his Ph.D. from Beijing Institute of Technology (BIT), P.R. China in January 2016. Currently, he is working as an Assistant Professor, department of mathematics, at COMSATS University Islamabad, Pakistan. His research interests include mathematical modeling & optimization, quality & reliability engineering, survival analysis, spatial data analysis, and data science. He has more than 10 research papers in reputed journals and proceedings of international conferences. Most recently he received National Research Program for Universities award from HEC Pakistan.

YASAR AMIN received the BSc degree in Electrical Engineering with specialization in Telecommunication and MBA in Innovation and Growth from Turku School of Economics, University of Turku, Finland. His MSc is in Electrical Engineering with specialization in System on Chip Design, and also Ph.D. is in Electronic and Computer Systems from Royal Institute of Technology (KTH), Sweden, with the research focus on printable green RFID antennas for embedded sensors. He is currently an Associate professor and chairman of Telecommunication Engineering Department, University of Engineering and Technology Taxila, Pakistan. He also serves as the Director of Embedded Systems Research and Development Centre. He is the founder of ACTSENA (Agile Creative Technologies for Smart Electromagnetic Novel Applications) research group. He has authored or co-authored more than 100 international technical papers in conferences and journals. His research interests include the design and application of multiple antenna systems for next generation mobile communication systems, millimeter-wave and terahertz antenna array, implantable & wearable electronics, and inkjet printing technology in microwave applications. He is a member of more than a dozen international professional societies and the fellow of PAE.

JONATHAN LOO received his MSc degree in Electronics from the University of Hertfordshire, UK in 1998 and his Ph.D. degree in Electronics and Communications from the same university in 2003. He leads a research team of 8 Ph.D. students in the area of communication and networking. He is presently Professor and Chair in Computing and Communication Engineering in School of Computing and Engineering University of West London, UK. His research interest includes network architecture, communication protocols, network security, embedded systems, video coding and transmission, wireless communications, digital signal processing, and optical networks. He has successfully graduated 13 PhDs as Principle Supervisor and contributed over 175 publications in the aforementioned specialist areas.

HANNU TENHUNEN is Chair Professor of Electronic Systems at Royal Institute of Technology (KTH), Stockholm, Sweden. He has been full professor, invited professor or visiting honorary professor in Finland (TUT, UTU), Sweden (KTH), USA (Cornel U), France (INPG), China (Fudan and Beijing Jiaotong Universities), and Hong Kong (Chinese University of Hong Kong), and has an honorary doctorate from Tallinn Technical University. He has been the director of multiple national large-scale research programs or being an initiator and director of national or European graduate schools. He has actively contributed to VLSI and SoC design in Finland and Sweden via creating new educational programs and research directions, most lately at European level as being the EU-level Education Director of the new European flagship initiative European Institute of Technology and Innovations (EIT), and its Knowledge and Innovation Community EIT ICT Labs. He is the founding editorial board member of 3 scientific journals and guest editor for multiple special issues of scientific journals and books. He has authored or co-authored more than 900 international technical papers in conferences and journals. He has been granted 9 foreign patents he is a member of Academy of Engineering Science of Finland.

• • •